Cerebral Cortex January 2009;19:72–78
doi:10.1093/cercor/bhn059
Advance Access publication April 9, 2008

Resting-State Functional Connectivity Reflects Structural Connectivity in the Default Mode Network

Michael D. Greicius[1,3], Kaustubh Supekar[4], Vinod Menon[2,3] and Robert F. Dougherty[5]

[1]Department of Neurology, Stanford University School of Medicine, Stanford, CA 94304, USA, [2]Department of Psychiatry, Stanford University School of Medicine, Stanford, CA 94304, USA, [3]Program in Neuroscience, Stanford University, Stanford, CA 94304, USA, [4]Department of Biomedical Informatics, Stanford University School of Medicine, Stanford, CA 94304, USA and [5]Department of Psychology, Stanford University, Stanford, CA 94304, USA

Resting-state functional connectivity magnetic resonance imaging (fcMRI) studies constitute a growing proportion of functional brain imaging publications. This approach detects temporal correlations in spontaneous blood oxygen level–dependent (BOLD) signal oscillations while subjects rest quietly in the scanner. Although distinct resting-state networks related to vision, language, executive processing, and other sensory and cognitive domains have been identified, considerable skepticism remains as to whether resting-state functional connectivity maps reflect neural connectivity or simply track BOLD signal correlations driven by nonneural artifact. Here we combine diffusion tensor imaging (DTI) tractography with resting-state fcMRI to test the hypothesis that resting-state functional connectivity reflects structural connectivity. These 2 modalities were used to investigate connectivity within the default mode network, a set of brain regions—including medial prefrontal cortex (MPFC), medial temporal lobes (MTLs), and posterior cingulate cortex (PCC)/retropslenial cortex (RSC)—implicated in episodic memory processing. Using seed regions from the functional connectivity maps, the DTI analysis revealed robust structural connections between the MTLs and the retrosplenial cortex whereas tracts from the MPFC contacted the PCC (just rostral to the RSC). The results demonstrate that resting-state functional connectivity reflects structural connectivity and that combining modalities can enrich our understanding of these canonical brain networks.

Keywords: Alzheimer's disease, hippocampus, memory, posterior cingulate, retrosplenial, white matter

Analyses of resting-state functional magnetic resonance imaging (fMRI) data have demonstrated temporal correlations in the blood oxygen level–dependent (BOLD) signal of widely separated brain regions (Biswal et al. 1995; Cordes et al. 2001). These temporal correlations are presumed to reflect intrinsic functional connectivity and have been demonstrated across several distinct networks serving critical functions like vision, hearing, language, and salience detection (Hampson et al. 2002; Beckmann et al. 2005; Seeley et al. 2007). One such network that has been studied extensively is the default mode network (DMN), a set of brain regions that typically deactivate during performance of cognitive tasks (Raichle et al. 2001). The DMN is detectable using task-free functional connectivity MRI and has been implicated in episodic memory processing (Greicius et al. 2003; Greicius et al. 2004; Buckner et al. 2005). Despite the growing number of resting-state functional connectivity MRI (fcMRI) studies, critical concerns regarding the underlying source of the BOLD signal correlations remain. Several groups have demonstrated that physiologic noise can contaminate the low-frequency oscillations on which fcMRI studies depend (Cordes et al. 2001; Birn et al. 2006; Shmueli et al. 2007). Given the various sources of noise that can contaminate these low-frequency BOLD signal oscillations, healthy skepticism persists as to how closely fcMRI estimates neural connectivity (Maldjian 2001).

Structural connections between brain regions are readily identified in nonhuman primates using tract-tracing methods. Most such studies are undertaken in macaques (Suzuki and Amaral 1994; Morris et al. 1999; Lavenex et al. 2002; Kobayashi and Amaral 2003; Parvizi et al. 2006). Similar studies in humans are not feasible because the most effective tracers require antemortem injections. Postmortem tract tracing in humans is severely restricted by the glacial pace of postmortem tracers and the limited distance they travel (Sparks et al. 2000). Thus, most assumptions about human brain connectivity are extrapolated from tracer studies in monkeys. Tracts connecting several nodes in the DMN have been demonstrated between the homologous regions in macaques. The medial temporal lobe (MTL) and the posterior cingulate cortex/retrosplenial cortex (PCC/RSC) are known to have monosynaptic connections (Suzuki and Amaral 1994; Morris et al. 1999; Lavenex et al. 2002; Kobayashi and Amaral 2003). These MTL–RSC tracts have been invoked in humans to explain why Alzheimer's disease patients show reduced metabolism in the PCC/RSC even in early stages where pathology is limited to the MTL (Greicius et al. 2004). Tracts between the PCC and the medial prefrontal cortex (MPFC) have also been demonstrated in macaques (Parvizi et al. 2006). The uncinate fasiculus has been shown in macaques to connect the anterior MTL with the more inferior, orbitofrontal aspect of the MPFC (Carmichael and Price 1995; Petrides and Pandya 2007).

The relationship between resting-state fcMRI and structural connectivity has not been explored in detail. A study of fcMRI in patients with agenesis of the corpus callosum showed little to no functional connectivity between the auditory cortices in the left and right hemisphere; a null finding suggesting that structural neural connections are required for functional connectivity (Quigley et al. 2003). Recent advances in diffusion tensor imaging (DTI) have allowed noninvasive in vivo measurement of white matter pathways in individual humans (Conturo et al. 1999; Mori et al. 1999; Basser et al. 2000; Catani et al. 2002; Behrens et al. 2003; Dougherty et al. 2005). One prior study (Koch et al. 2002) found that DTI structural connectivity measures between adjacent gyri correlated with task-free functional connectivity measures. This relationship has not been examined across nonadjacent regions in whole-brain networks. The poor temporal resolution of fMRI precludes determining whether functional connectivity between 2 nodes reflects a direct (potentially monosynaptic)

connection or is conducted across multiple synapses via intervening nodes. Here, we combined DTI tractography and resting-state fMRI to test the general hypothesis that resting-state functional connectivity reflects structural connectivity. Based on the tract-tracing data in macaques, we hypothesized more specifically that direct connections between PCC and MTL and between PCC and MPFC would be detectable whereas direct connections between MPFC and MTL would not.

Methods

Subjects

Twenty-three healthy young subjects (7 women) aged 19–45 years (mean 29 years) participated in this study. Six of these subjects aged 23–37 years (2 women) underwent both the fMRI and DTI portion of the study. All subjects were physically healthy and had no significant history of neurological disease, psychiatric disease, or head injury. The Stanford Panel on Human Subjects in Medical and Non-Medical Research approved all procedures. Written informed consent was obtained from all participants.

DTI and fMRI data were acquired on 1.5T Signa LX (Signa CVi, GE Medical Systems, Milwaukee, WI) using a self-shielded, high-performance gradient system capable of providing a maximum gradient strength of 50 mT/m at a gradient rise time of 268 μs for each of the gradient axes. A standard quadrature head coil, provided by the vendor, was used for excitation and signal reception. Head motion was minimized by placing cushions around the head and securing a Velcro strap across the forehead.

Functional MRI

Six subjects underwent an 8-min, task-free spiral in/out functional scan (Glover and Law 2001) with the following parameters: time repetition (TR) = 2.5 s; time echo (TE) = 40 ms; flip angle = 85°; slice thickness = 4 mm; skip = 1 mm; 30 slices. Subjects were instructed simply to close their eyes and hold still.

After discarding the first 4 volumes to allow for stabilization of the magnetic field, the images were concatenated across time into a single 4-dimensional image. The 4-dimensional image was then spatially smoothed with an 8-mm kernel, temporally filtered with a 100-s high pass filter, and subjected to independent component analysis (ICA) with FSL's melodic software (www.fmrib.ox.ac.uk/fsl/melodic2/index.html). ICA is a statistical technique that separates a set of signals into independent—uncorrelated and non-Gaussian—spatiotemporal components (Beckmann and Smith 2004). When applied to the T2* signal of fMRI, ICA allows not only for the removal of artifact (McKeown et al. 1998; Quigley et al. 2002) but also for the isolation of task-activated neural networks (McKeown et al. 1998; Gu et al. 2001; Calhoun et al. 2002). Most recently, ICA has been used to identify neural networks, including the DMN, during task-free or cognitively undemanding fMRI scans (Greicius et al. 2004; van de Ven et al. 2004; Beckmann et al. 2005). We allowed the software to estimate the optimal number of components for each subject. All components were then transformed into standard MNI space, and the DMN component was selected from among each subject's independent components using an automated template-matching procedure as we have done previously (see Fig. 1 in (Greicius et al. 2007). This procedure includes a frequency filter step that excludes any components in which 50% or more of the power in the frequency domain is above 0.1 Hz.

After selecting the best-fit DMN component, the native space DMN component for each subject was aligned to the custom template space in which the DTI analyses were performed (described below). This was done by aligning T2-weighted images acquired in the same session and with the same prescription as the fMRI data to that subject's T1-weighted 3D SPGR anatomical image volume using a mutual information 3-D rigid-body coregistration algorithm from SPM2 (Ashburner and Friston 2003). The spatial normalization parameters that map each individual brain to the custom template were computed based on the T1-weighted images. A one-sample *t*-test was performed with SPM2 on the normalized DMN maps. Significant clusters in the resulting group-level map were determined using a joint probability threshold (Poline et al. 1997) of $P < 0.001$ (height and extent, corrected) and a minimum cluster size of 100 voxels (Fig. 1A). Regions of interest (ROIs) were selected from

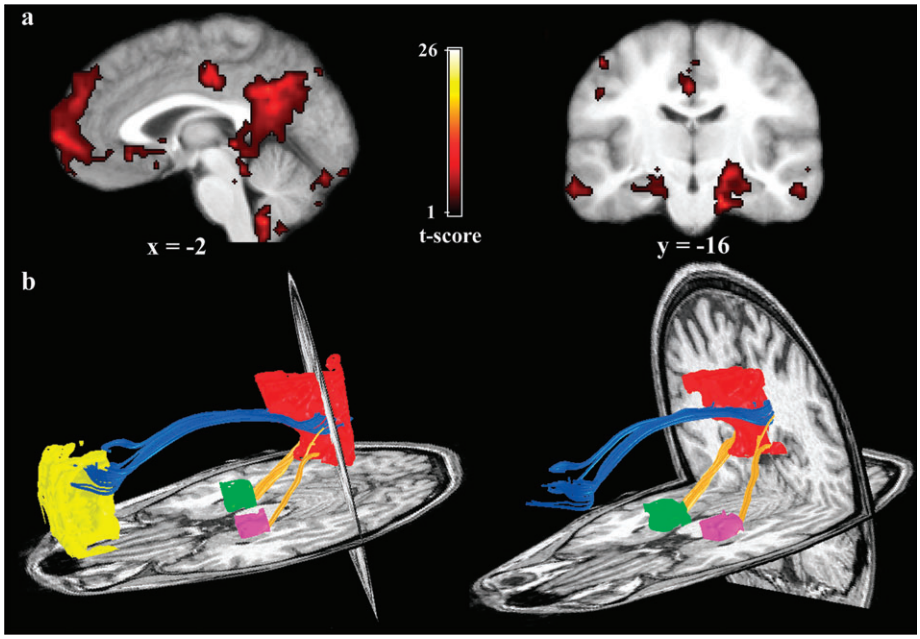

Figure 1. Functional connectivity reflects structural connectivity in the DMN. (*a*) Task-free, functional connectivity in the DMN is shown in a group of 6 subjects. The PCC/RSC and MPFC clusters are best appreciated on the sagittal view. Prominent bilateral MTL clusters are seen on the coronal image (left side of image corresponds to left side of brain). (*b*) DTI fiber tractography in a single subject demonstrates the cingulum bundle (blue tracts) connecting the PCC/RSC to the MPFC. The yellow tracts connect the bilateral MTL to the PCC/RSC. Note that generally the tracts from the MPFC enter the more rostral aspect of the PCC/RSC ROI corresponding to the PCC proper, whereas the tracts from MTL enter the more caudal aspect of the PCC/RSC ROI corresponding to the RSC proper. Left and right columns show slightly different views of the same tracts to highlight the distinct entry points into the PCC/RSC. There were no tracts connecting the MPFC to the MTL.

clusters in the MPFC, PCC/RSC, and MTL bilaterally. After visually selecting a one-voxel seed-point within each cluster on the functional map, the final ROIs were grown around the seed-point using an in-house 3-D flood-fill algorithm. The algorithm grew a spatially contiguous ROI by beginning with the seed point and filling all connected voxels with a t statistic that was within 20% of that of the seed voxel. For the smaller MTL ROI, we also limited the radius of the 3-D flood-fill algorithm to a maximum of 25 mm from the seed voxel to prevent the ROI from extending beyond the MTL region. These 4 group-level, spatially normalized ROIs obtained from the fMRI data were then warped back to each individual brain so that they could be used for the subsequent DTI tractography analyses. This was done by applying the inverse of the spatial normalization transformation. As fiber tracking becomes unreliable in gray matter, we ensured that our ROIs extended 2–3mm into the white matter.

Diffusion Tensor Imaging

The DTI protocol used eight 90-s whole-brain scans averaged to improve signal quality. The pulse sequence was a diffusion-weighted single-shot spin-echo, echo planar imaging sequence (TE = 63 ms; TR = 6 s; field of view = 260 mm; matrix size = 128 × 128; bandwidth = ±110kHz; partial k-space acquisition). We acquired 56 axial, 2-mm thick slices (no skip) for 2 b values, b = 0 and b = approximately 800 s/mm^2. The high b value was obtained by applying gradients along 12 different diffusion directions (six noncollinear directions). Two gradient axes were energized simultaneously to minimize TE. The polarity of the effective diffusion-weighting gradients was reversed for odd repetitions to reduce cross-terms between diffusion gradients and imaging and background gradients. Although Jones (2004) suggests that measuring more diffusion directions would be a more efficient way to reliably estimate diffusion tensors of arbitrary orientation, our signal-to-noise ratio is sufficiently high from our 8 repeats to produce very reliable tensor estimates suitable for tractography. We have confirmed this in a subset of subjects by comparing 60-direction data with the 12-direction data reported here.

DTI data were preprocessed using a custom program based on normalized mutual information that removed eddy current distortion effects and determined a constrained nonrigid image registration of all the diffusion images (Bammer et al. 2002). The 6 elements of the diffusion tensor were determined by multivariate regression (Basser 1995; Basser and Pierpaoli 1996). For each subject, the non–diffusion-weighted (b = 0) images were coregistered to the T1-weighted 3-D SPGR anatomical images using a mutual information 3-D rigid-body coregistration algorithm from SPM2 (Ashburner and Friston 2003). Several anatomical landmarks, including the anterior commissure (AC), the posterior commissure (PC), and the midsagittal plane, were identified by hand in the T1 images. With these landmarks, we computed a rigid-body transform from the native image space to the conventional AC-PC–aligned space. The DTI data were then resampled to this AC-PC–aligned space with 2-mm isotropic voxels using a spline-based tensor interpolation algorithm (Pajevic et al. 2002), taking care to rotate the tensors to preserve their orientation with respect to the anatomy (Alexander et al. 2001). The T1 images were resampled to AC-PC–aligned space with 1-mm isotropic voxels. We confirmed by visual inspection of each dataset that this coregistration technique aligns the DTI and T1 images to within 1–2 millimeters in the brain regions of interest.

DTI fiber tractography was used to estimate the likely connections between the 4 ROIs. Using custom DTI analysis software (available for download at http://sirl.stanford.edu/software/), the tractography procedure was initiated by whole-brain fiber tracking that produced many fiber paths. Tracts that did not end in or pass through both ROIs were discarded. For the smaller MTL ROIs, tracts were kept if they ended in or passed through the ROI; for the larger MPFC and PCC/RSC ROIs, tracts were kept only if they ended in the ROI. "End in" is a stricter criterion than "pass through" and discards fibers that merely graze the ROI en route to other cortical regions. This is particularly important if an ROI extends into the white matter where there is a risk of catching unrelated fibers passing by the ROI. Each fiber tract was estimated using a deterministic streamlines tracking algorithm (Conturo et al. 1999; Mori et al. 1999; Basser et al. 2000) with a fourth order Runge-Kutta path integration method (Press et al. 2002) and 1 mm fixed step size. A continuous tensor field was estimated using trilinear interpolation of the tensor elements. Starting from the initial seed point, fiber paths were traced in both directions along the principal diffusion axis. Path tracing proceeded until the FA fell below 0.15 or until the minimum angle between the current and previous path segments was larger than 30°. Given the risk of false negatives in DTI tractography and the lack of standard criteria for thresholding tracts, we performed a secondary analysis in which we loosened these criteria allowing path tracing to proceed until the minimum angle between segments exceeded 90°. To limit the number of false positives, fibers that were anatomically implausible were identified visually and removed. This was not done when searching for fibers between the MPFC and MTL ROIs so that we could more rigorously test our hypothesis that there would be no fibers between these ROIs. To combine resulting fiber maps, individual tracts were translated into a common space by applying the spatial normalization parameters that map each individual brain to the same custom template to which the fMRI data were aligned. This template was created from 20 normal adult brains (including 3 of the 6 fMRI participants and 17 of the additional DTI participants) using standard nonlinear spatial normalization methods from SPM2. The deformation field resulting from the spatial normalization calculation was applied to the fiber coordinates from each individual brain to bring them all into a common space. Cross-subject connection maps in the common space were generated by counting, in each voxel, the number of subjects who have a fiber passing through that voxel. Additional methods details are available in a previous publication (Dougherty et al. 2005).

Results

Figure 1A shows the DMN resting-state connectivity map from which the ROIs were taken. Single-subject tracts connecting the PCC/RSC to the MPFC and MTL are shown in Figure 1B. The MTL fibers generally enter the caudal, retrosplenial portion of the PCC/RSC ROI, whereas the MPFC fibers enter the more rostral (PCC proper) portion of this ROI. This rostral–caudal distinction—MPFC–PCC/RSC tracts entering the PCC proper and MTL–PCC/RSC fibers entering the more caudal RSC—was a consistent finding across individual subjects (Fig. 2). There were no tracts connecting the MPFC to the MTL.

The group-level map of the tracts is shown in Figure 3 using a subject count threshold. Voxels with tracts from fewer than 5 subjects are not colored. The tracts connecting PCC/RSC to MPFC were detected in 22 of 23 subjects, and those connecting PCC/RSC to MTL were detected in all 23 subjects (to both left and right MTL ROIs). Although these tracts were detected in 22 to 23 of 23 subjects, the fiber density maps in Figure 3 show voxel values less than 22 due to the individual variability in the precise path of the tracts from one voxel to the next. As with the single-subject tracts, the group-level map shows that fibers from the MTL enter the more caudal, putative retrsoplenial, portion of the PCC/RSC ROI, whereas the fibers from the MPFC enter the more rostral aspect corresponding to the PCC proper. There were no tracts connecting the MPFC and MTL using this group-level method and at the single-subject level tracts connecting MPFC to MTL were found in none of the 23 subjects. Given the risk of false negatives in DTI, we repeated the search for MPFC–MTL tracts using substantially looser angle thresholds but again detected none.

Discussion

We combined resting-state fcMRI with DTI to demonstrate that resting-state functional connectivity reflects, to a large degree, the underlying structural connectivity. This finding, coupled with work in patients with agenesis of the corpus callosum

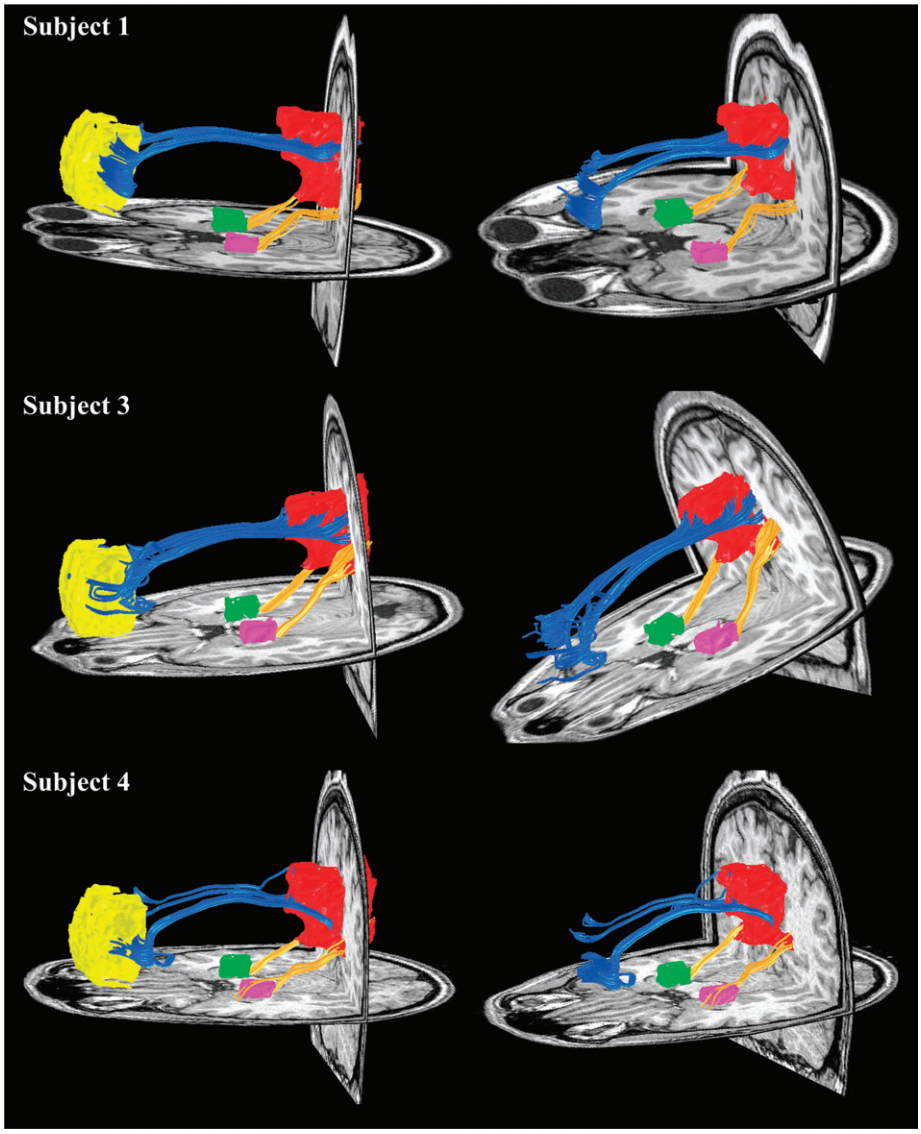

Figure 2. DTI fiber tractography in 3 additional subjects. In all cases, the MPFC fibers (blue tracts) enter the rostral (PCC proper) aspect of the PCC/RSC ROI, whereas the MTL fibers (yellow tracts) enter the more caudal aspect (RSC proper) of the PCC/RSC ROI. Left and right columns show slightly different views of the same tracts to highlight the distinct entry points into the PCC/RSC. There were no tracts connecting the MPFC to the MTL.

(Quigley et al. 2003) should help refute some of the (healthy) skepticism surrounding resting-state fcMRI analyses (Maldjian 2001). Although physiologic noise from several sources can certainly contaminate the connectivity maps (Cordes et al. 2001; Birn et al. 2006; Shmueli et al. 2007) the preponderance of evidence now suggests that resting-state fcMRI is a marker of neural connectivity.

Several lines of evidence suggest that the particular network investigated here, the DMN, plays a vital role in episodic memory processing. First, it includes bilateral hippocampus clusters both in humans and macaques (Greicius 2004; Vincent et al. 2007). Second, although deactivated by most cognitive tasks, it is activated by episodic memory tasks (Maguire and Mummery 1999; Buckner et al. 2005). Finally, it overlaps considerably with brain regions targeted by Alzheimer's disease (Greicius et al. 2004; Buckner et al. 2005), the quintessential disorder of episodic memory. By isolating tracts within the DMN connecting the RSC to the MTL, the current study adds to the evidence linking the DMN to episodic memory. These RSC–MTL pathways have been identified in macaque tracer studies but not previously shown explicitly in humans. We suspect that the tracts shown here are a subset of the descending cingulum bundle demonstrated in previous studies (Wakana et al. 2004; Concha, Beaulieu, et al. 2005; Concha, Gross, et al. 2005). Those earlier studies used manually selected ROIs drawn in white matter to define tracts and did not explicitly define terminal connections. By contrast, in the current study, we used functional ROIs in the cortex and hippocampus and defined terminal connections in cortex by using an "end-in" criterion. In addition to the RSC–MTL tracts demonstrated here, the descending cingulum bundle likely encompasses other tracts connecting the PCC/RSC with regions in the lateral temporal lobe and thalamus (Morris et al. 1999).

The caudal entry point of MTL fibers into the PCC/RSC (compared with the more rostral entry of MPFC fibers) is consistent with monkey studies showing that RSC (as opposed

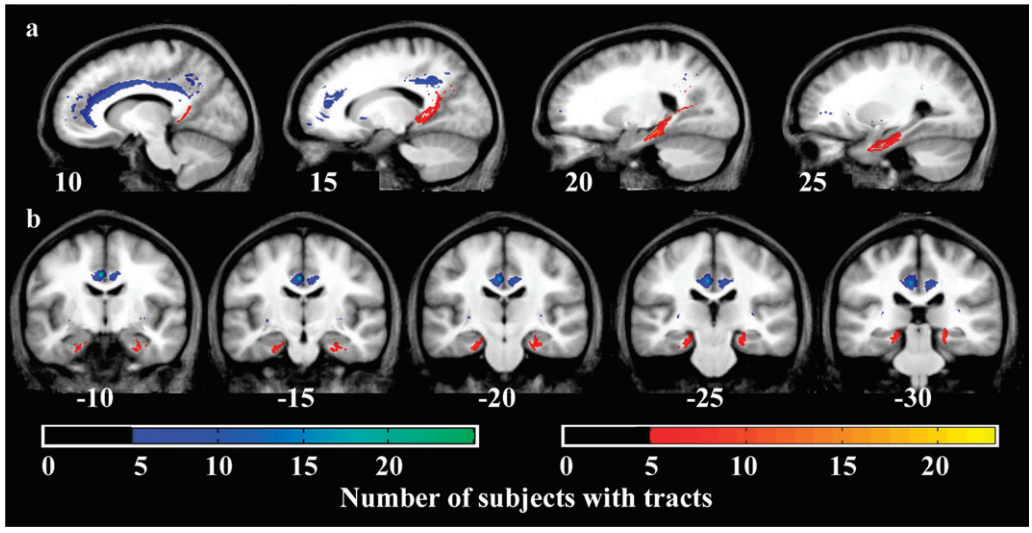

Figure 3. Tracts are consistent across subjects. (*a*) Sagittal views of the MPFC–PCC/RSC tracts (blue–green) and MTL–PCC/RSC tracts (red–yellow) where the color scales indicate the number of subjects that had a tract in a given voxel. The more medial sagittal views at $x = 10$ and $x = 15$ demonstrate the distinct entry points of the 2 tracts into the PCC/RSC with the MPFC fibers entering rostrally and the MTL fibers entering caudally. (*b*) Coronal views show the red–yellow MTL fibers coursing between the hippocampus and parahippocampal gyrus (whose anterior extent at $y = -10$ includes entorhinal cortex). There were no tracts connecting the MPFC to the MTL.

to PCC proper) is densely connected with MTL (Suzuki and Amaral 1994; Morris et al. 1999; Lavenex et al. 2002; Kobayashi and Amaral 2003). Our MTL ROIs contain hippocampus proper as well as the inferiorly adjacent parahippocampal and entorhinal cortex. On coronal sections (Fig. 3), the tracts appear to course along the white matter between the hippocampus and the parahippocampus (posteriorly) and entorhinal cortex (anteriorly). As such, we cannot distinguish which subregions of MTL are most densely connected with the RSC. We would predict, from work in macaques, that the bulk of the connectivity is via the entorhinal cortex but tracer studies have also shown direct projections between RSC and hippocampus (Kobayashi and Amaral 2003). Future studies creating ROIs from MTL subregions should enable still more detailed mapping of these tracts, but precise mapping will require higher resolution diffusion data to resolve the exact location at which fibers turn to enter the gray matter.

DTI tractography, as used here in conjunction with resting-state fMRI, has the potential to enrich our understanding of human functional networks. Although functional connectivity implies structural connectivity, it cannot distinguish between direct (potentially monosynaptic) and indirect (potentially multisynaptic) connections. We have demonstrated, for example, that within the DMN the PCC/RSC appears to have direct projections to the MPFC and MTL, whereas the MTL and MPFC appear not to have direct connections. The uncinate fasciculus has been shown to connect the MTLs to the inferior aspect of the MPFC (Wakana et al. 2004) but not to the more superior MPFC region examined here. One must be wary of false negatives, especially in tractography studies. However, the majority of known false negatives in tractography studies involve small, laterally running tracts that are lost when crossing larger tracts like the longitudinal fasciculii and corona radiata (Dougherty et al. 2005). Further, in a post hoc analysis, we loosened our path-tracing thresholds substantially and were still unable to detect tracts connecting our MTL and MPFC ROIs. As such, the absence of connections here between the medially located MPFC and MTL likely reflects a true negative, suggesting that functional connections between these 2 nodes are mediated via a third party such as the PCC/RSC.

The tractography results also point to the coarseness of functional connectivity maps when considered in isolation. The DMN identified here includes a large functional cluster that probably collapses 2 distinct functional regions, the PCC and the RSC, into a single PCC/RSC cluster. The DTI data, showing tracts from the MTL entering caudally into the RSC and tracts from the MPFC entering rostrally into the PCC, certainly suggest that these adjacent regions have distinct projections. In this instance, the DTI results have the potential to better outline the hierarchy of connectivity in the DMN and suggest that there is a flow of information from MTL to RSC to the adjacent PCC to the MPFC. In these data, the functional and structural connections from RSC to the adjacent PCC cannot be shown but must instead be assumed. Evidence from a recent ROI-based study (see figure 5b in Vincent et al. [2006]) supports this distinction between RSC and PCC connectivity by showing that RSC–MTL connections are stronger than PCC–MTL connections, though the latter were also detectable. Future work with both ICA and ROI-based studies should help further delineate the detailed functional and structural architecture of the DMN. It would be informative, for example, to see if forcing ICA to generate more components would result in a splitting of the DMN into 2 or more subnetworks. The hypothesized functional path from MTL to RSC to PCC to MPFC could also be assessed by directly contrasting ROI-based maps of PCC and RSC connectivity using a paired *t*-test.

In describing the relationship between functional and structural connectivity in this study, we have been careful to note that functional connectivity "reflects" structural connectivity. As our results demonstrate, although functional connectivity reflects structural connectivity to a large degree there is not a simple one-to-one mapping. This is most evident in the lack of MPFC–MTL tracts described above strongly supporting the intuitive notion that functional connectivity can exist in the

absence of direct, monosynaptic connections. The converse, that structural connectivity can exist in the absence of functional connectivity, is less intuitive and not addressed by our data but nonetheless quite plausible. Perhaps the best example of this scenario relates to context-dependent changes in connectivity. Several groups have demonstrated that functional connectivity between regions with known or presumed structural connections can wax or wane depending on contextual variables such as awareness of learning (McIntosh et al. 2003) or task performance (Hampson et al. 2004; Rissman et al. 2004). In sum, although our data show that resting-state functional connectivity reflects structural connectivity to a large degree, each can exist without the other.

The main limitation of our study is that our survey of the DMN was incomplete in that we were not able to interrogate the structural connectivity of the bilateral angular gyri. Our group (Greicius et al. 2003) and others (Vincent et al. 2006) have shown that the bilateral angular gyri are key nodes in the DMN. Unfortunately, our ability to examine tracts running laterally to and from the angular gyrus is severely restricted owing to the problem of resolving crossing fibers in tractography analyses (Mori and Zhang 2006; Peled et al. 2006). Although it is quite likely that there are direct connections between the angular gyrus and the PCC (and perhaps to the MTL and MPFC), we assumed, a priori, that these smaller laterally running fibers would be impossible to trace through the larger perpendicularly oriented tracts like the anterior-to-posterior oriented superior longitudinal fasiculus and the superior-to-inferior oriented corona radiata (Dougherty et al. 2005). This assumption was confirmed in an analysis (data not shown) in which we were only able to find tracts connecting the PCC to the angular gyrus in 4 of 23 subjects, tracts connecting the MPFC to the angular gyrus in 4 of 23 subjects, and tracts connecting the MTL to the angular gyrus in 2 of 23 subjects. Future work using novel algorithms designed to overcome the problem of crossing fibers (Peled et al. 2006) will hopefully allow for a more complete investigation of structural connectivity in the DMN and other functional networks.

Subsequent, more detailed, applications of combined DTI tractography and functional connectivity MRI to both controls and patient groups should greatly enhance our understanding of functional (and dysfunctional) brain networks. To cite a specific example, independent groups have already shown that functional (Greicius et al. 2004) and structural (Zhang et al. 2007) measures of DMN connectivity have potential utility in distinguishing Alzheimer's disease patients from controls. Rather than examining these DMN measures in isolation, the current findings suggest that combining structural and functional approaches in the same subjects should ultimately allow for superior characterization of the DMN changes caused by Alzheimer's disease (Buckner et al. 2005).

Funding

Alzheimer's Association (NIRG-04-1060); National Science Foundation (BCS-0449927); National Institutes of Health (NS048302, EY015000, HD047520, NS058899).

Notes

Conflict of Interest: None declared.

Address correspondence to Michael D. Grecius, MD 300 Pasteur Drive, Room A343 Stanford, CA 94305-5235. Email: greicius@stanford.edu.

References

Alexander DC, Pierpaoli C, Basser PJ, Gee JC. 2001. Spatial transformations of diffusion tensor magnetic resonance images. IEEE Trans Med Imaging. 20:1131–1139.

Ashburner J, Friston KJ. 2003. Human Brain Function. New York: Academic.

Basser PJ. 1995. Inferring microstructural features and the physiological state of tissues from diffusion-weighted images. NMR Biomed. 8: 333–344.

Basser PJ, Pajevic S, Pierpaoli C, Duda J, Aldroubi A. 2000. In vivo fiber tractography using DT-MRI data. Magn Reson Med. 44: 625–632.

Basser PJ, Pierpaoli C. 1996. Microstructural and physiological features of tissues elucidated by quantitative-diffusion-tensor MRI. J Magn Reson B. 111:209–219.

Beckmann CF, DeLuca M, Devlin JT, Smith SM. 2005. Investigations into resting-state connectivity using independent component analysis. Philos Trans R Soc Lond B Biol Sci. 360:1001–1013.

Beckmann CF, Smith SM. 2004. Probabilistic independent component analysis for functional magnetic resonance imaging. IEEE Trans Med Imaging. 23:137–152.

Behrens TE, Johansen-Berg H, et al. 2003. Non-invasive mapping of connections between human thalamus and cortex using diffusion imaging. Nat Neurosci. 6:750–757.

Birn RM, Diamond JB, Smith MA, Bandettini PA. 2006. Separating respiratory-variation-related fluctuations from neuronal-activity-related fluctuations in fMRI. Neuroimage. 31:1536–1548.

Biswal B, Yetkin FZ, Haughton VM, Hyde JS. 1995. Functional connectivity in the motor cortex of resting human brain using echo-planar MRI. Magn Reson Med. 34:537–541.

Buckner RL, Snyder AZ, et al. 2005. Molecular, structural, and functional characterization of Alzheimer's disease: evidence for a relationship between default activity, amyloid, and memory. J Neurosci. 25: 7709–7717.

Calhoun VD, Pekar JJ, McGinty VB, Adali T, Watson TD, Pearlson GD. 2002. Different activation dynamics in multiple neural systems during simulated driving. Hum Brain Mapp. 16:158–167.

Carmichael ST, Price JL. 1995. Limbic connections of the orbital and medial prefrontal cortex in macaque monkeys. J Comp Neurol. 363:615–641.

Catani M, Howard RJ, Pajevic S, Jones DK. 2002. Virtual in vivo interactive dissection of white matter fasciculi in the human brain. Neuroimage. 17:77–94.

Concha L, Beaulieu C, Gross DW. 2005. Bilateral limbic diffusion abnormalities in unilateral temporal lobe epilepsy. Ann Neurol. 57: 188–196.

Concha L, Gross DW, Beaulieu C. 2005. Diffusion tensor tractography of the limbic system. AJNR Am J Neuroradiol. 26:2267–2274.

Conturo TE, Lori NF, Cull TS, Akbudak E, Snyder AZ, Shimony JS, McKinstry RC, Burton H, Raichle ME. 1999. Tracking neuronal fiber pathways in the living human brain. Proc Natl Acad Sci U S A. 96: 10422–10427.

Cordes D, Haughton VM, Arfanakis K, Carew JD, Turski PA, Moritz CH, Quigley MA, Meyerand ME. 2001. Frequencies contributing to functional connectivity in the cerebral cortex in "resting-state" data. AJNR Am J Neuroradiol. 22:1326–1333.

Dougherty RF, Ben-Shachar M, Bammer R, Brewer AA, Wandell BA. 2005. Functional organization of human occipital-callosal fiber tracts. Proc Natl Acad Sci U S A. 102:7350–7355.

Glover GH, Law CS. 2001. Spiral-in/out BOLD fMRI for increased SNR and reduced susceptibility artifacts. Magn Reson Med. 46:515–522.

Greicius MD, Flores BH, Menon V, Glover GH, Solvason HB, Kenna H, Reiss AL, Schatzberg AF. 2007. Resting-state functional connectivity in major depression: abnormally increased contributions from subgenual cingulate cortex and thalamus. Biol Psychiatry. 62: 429–437.

Greicius MD, Krasnow B, Reiss AL, Menon V. 2003. Functional connectivity in the resting brain: a network analysis of the default mode hypothesis. Proc Natl Acad Sci U S A. 100:253–258.

Greicius MD, Srivastava G, Reiss AL, Menon V. 2004. Default-mode network activity distinguishes Alzheimer's disease from healthy

aging: evidence from functional MRI. Proc Natl Acad Sci U S A. 101: 4637–4642.
Gu H, Engelien W, Feng H, Silbersweig DA, Stern E, Yang Y. 2001. Mapping transient, randomly occurring neuropsychological events using independent component analysis. Neuroimage. 14: 1432–1443.
Hampson M, Olson IR, Leung HC, Skudlarski P, Gore JC. 2004. Changes in functional connectivity of human MT/V5 with visual motion input. Neuroreport. 15:1315–1319.
Hampson M, Peterson BS, Skudlarski P, Gatenby JC, Gore JC. 2002. Detection of functional connectivity using temporal correlations in MR images. Hum Brain Mapp. 15:247–262.
Jones DK. 2004. The effect of gradient sampling schemes on measures derived from diffusion tensor MRI: a Monte Carlo study. Magn Reson Med. 51:807–815.
Kobayashi Y, Amaral DG. 2003. Macaque monkey retrosplenial cortex: II. Cortical afferents. J Comp Neurol. 466:48–79.
Koch MA, Norris DG, Hund-Georgiadis M. 2002. An investigation of functional and anatomical connectivity using magnetic resonance imaging. Neuroimage. 16:241–250.
Lavenex P, Suzuki WA, Amaral DG. 2002. Perirhinal and parahippocampal cortices of the macaque monkey: projections to the neocortex. J Comp Neurol. 447:394–420.
Maguire EA, Mummery CJ. 1999. Differential modulation of a common memory retrieval network revealed by positron emission tomography. Hippocampus. 9:54–61.
Maldjian JA. 2001. Functional connectivity MR imaging: fact or artifact? AJNR Am J Neuroradiol. 22:239–240.
McIntosh AR, Rajah MN, Lobaugh NJ. 2003. Functional connectivity of the medial temporal lobe relates to learning and awareness. J Neurosci. 23:6520–6528.
McKeown MJ, Jung TP, Makeig S, Brown G, Kindermann SS, Lee TW, Sejnowski TJ. 1998. Spatially independent activity patterns in functional MRI data during the stroop color-naming task. Proc Natl Acad Sci U S A. 95:803–810.
Mori S, Crain BJ, Chacko VP, van Zijl PC. 1999. Three-dimensional tracking of axonal projections in the brain by magnetic resonance imaging. Ann Neurol. 45:265–269.
Mori S, Zhang J. 2006. Principles of diffusion tensor imaging and its applications to basic neuroscience research. Neuron. 51:527–539.
Morris R, Petrides M, Pandya DN. 1999. Architecture and connections of retrosplenial area 30 in the rhesus monkey (Macaca mulatta). Eur J Neurosci. 11:2506–2518.
Pajevic S, Aldroubi A, Basser PJ. 2002. A continuous tensor field approximation of discrete DT-MRI data for extracting microstructural and architectural features of tissue. J Magn Reson. 154: 85–100.
Parvizi J, Van Hoesen GW, Buckwalter J, Damasio A. 2006. Neural connections of the posteromedial cortex in the macaque. Proc Natl Acad Sci U S A. 103:1563–1568.
Peled S, Friman O, Jolesz F, Westin CF. 2006. Geometrically constrained two-tensor model for crossing tracts in DWI. Magn Reson Imaging. 24:1263–1270.
Petrides M, Pandya DN. 2007. Efferent association pathways from the rostral prefrontal cortex in the macaque monkey. J Neurosci. 27: 11573–11586.
Poline JB, Worsley KJ, Evans AC, Friston KJ. 1997. Combining spatial extent and peak intensity to test for activations in functional imaging. Neuroimage. 5:83–96.
Press WH, Teukolsky SA, Vetterling WT, Flannery BP. 2002. Numerical Recipes in C++: The Art of Scientific Computing. Cambridge, U.K.: Cambridge University Press.
Quigley M, Cordes D, Turski P, Moritz C, Haughton V, Seth R, Meyerand ME. 2003. Role of the corpus callosum in functional connectivity. AJNR Am J Neuroradiol. 24:208–212.
Quigley MA, Haughton VM, Carew J, Cordes D, Moritz CH, Meyerand ME. 2002. Comparison of independent component analysis and conventional hypothesis-driven analysis for clinical functional MR image processing. AJNR Am J Neuroradiol. 23:49–58.
Raichle ME, MacLeod AM, Snyder AZ, Powers WJ, Gusnard DA, Shulman GL. 2001. A default mode of brain function. Proc Natl Acad Sci U S A. 98:676–682.
Rissman J, Gazzaley A, D'Esposito M. 2004. Measuring functional connectivity during distinct stages of a cognitive task. Neuroimage. 23:752–763.
Seeley WW, Menon V, Schatzberg AF, Keller J, Glover GH, Kenna H, Reiss AL, Greicius MD. 2007. Dissociable intrinsic connectivity networks for salience processing and executive control. J Neurosci. 27:2349–2356.
Shmueli K, van Gelderen P, de Zwart JA, Horovitz SG, Fukunaga M, Jansma JM, Duyn JH. 2007. Low-frequency fluctuations in the cardiac rate as a source of variance in the resting-state fMRI BOLD signal. Neuroimage. 38:306–320.
Sparks DL, Lue LF, Martin TA, Rogers J. 2000. Neural tract tracing using Di-I: a review and a new method to make fast Di-I faster in human brain. J Neurosci Methods. 103:3–10.
Suzuki WA, Amaral DG. 1994. Perirhinal and parahippocampal cortices of the macaque monkey: cortical afferents. J Comp Neurol. 350: 497–533.
van de Ven VG, Formisano E, Prvulovic D, Roeder CH, Linden DEJ. 2004. Functional connectivity as revealed by spatial independent component analysis of fMRI measurements during rest. Hum Brain Mapp. 22:165–178.
Vincent JL, Patel GH, et al. 2007. Intrinsic functional architecture in the anaesthetized monkey brain. Nature. 447:83–86.
Vincent JL, Snyder AZ, Fox MD, Shannon BJ, Andrews JR, Raichle ME, Buckner RL. 2006. Coherent spontaneous activity identifies a hippocampal-parietal memory network. J Neurophysiol. 96: 3517–3531.
Wakana S, Jiang H, Nagae-Poetscher LM, van Zijl PC, Mori S. 2004. Fiber tract-based atlas of human white matter anatomy. Radiology. 230: 77–87.
Zhang Y, Schuff N, Jahng GH, Bayne W, Mori S, Schad L, Mueller S, Du AT, Kramer JH, Yaffe K, Chui H, Jagust WJ, Miller BL, Weiner MW. 2007. Diffusion tensor imaging of cingulum fibers in mild cognitive impairment and Alzheimer disease. Neurology. 68:13–19.